

# Investigation on heat-affected zone hydrogen-induced cracking of high-strength naval steels using the Granjon implant test

HENRY GRANJON PRIZE 2014 Winner Category B: Materials Behaviour and Weldability

Xin Yue

Received: 3 May 2014 / Accepted: 11 June 2014 / Published online: 10 July 2014  
© International Institute of Welding 2014

**Abstract** The implant test was used to study the heat-affected zone (HAZ) hydrogen-induced cracking (HIC) susceptibility of a recently developed blast-resistant steel BlastAlloy 160 (BA-160) and two existing naval steels, HY-100 and HSLA-100. It was found that the coarse-grained HAZ (CGHAZ) is the most susceptible to HIC in the entire HAZ. Therefore, phase transformation behavior in the CGHAZ was investigated and continuous cooling transformation (CCT) diagrams for the CGHAZ of the three steels were developed. The new BA-160 steel was compared with the current steels HY-100 and HSLA-100 with respect to inherent resistance to HIC and sensitivity to diffusible hydrogen level based on the implant test results. Fracture surfaces of the implant specimens were also studied, which supports the implant test results when comparing the three steels. Different performance of the three steels is a result of the formation of different microstructures in the CGHAZ. In addition, the effect of welding parameters on reducing HIC tendency of BA-160 was studied using the implant test, providing recommendations for welding BA-160 when HIC is a big concern.

**Keywords** Heat-affected zone · Transformation · Hydrogen · Embrittlement · Implant tests · Fractography · High-strength steels

## 1 Introduction

Ship structures are subjected to a complex spectrum of dynamic loading in service and stresses in the hull as a result of fabrication and fit-up. Therefore, modern shipbuilding designs have shown a continuing trend of increasing application of high-strength steels, in order to achieve weight reduction, increased payload, and mobility. This will continue to be the trend in the foreseeable future, owing to the high strength and high fracture toughness of high-strength steels, which can assure the structural integrity of the hull and the use of steels can keep the production cost affordable [1–4].

Due to the excellent combination of high strength and toughness, steels like HY-100 and HSLA-100 are still being widely used in shipbuilding today; and the Navy is continuing to put great efforts into developing new high-performance steels [5–9]. The projected property requirement for future hull and deck steels is toughness above 115 J at  $-64\text{ }^{\circ}\text{C}$  with a yield strength in the range from 1,030 to 1,240 MPa. In addition, the new steels should possess good formability and weldability. A new steel, BlastAlloy 160 (BA-160) was designed by Northwestern University to meet these rigorous property requirement [10–12].

BA-160 steel was designed based on a theoretical computational materials design concept, using a multi-scale materials modeling method and advanced microstructural characterization techniques. The microstructure of BA-160 is a mixture of tempered martensite and bainite, with  $\text{M}_2\text{C}$  carbides (where  $\text{M}=\text{Cr}$ ,  $\text{Mo}$ , and  $\text{V}$ ) and copper precipitates dispersed in the matrix, which are in the range of 3–5 nm. The above carefully designed microstructure results in a high yield strength of 1,100 MPa (160 ksi). The high impact toughness of 176 J at  $25\text{ }^{\circ}\text{C}$  results from the presence of finely dispersed Ni-stabilized austenite in the microstructure, which toughens the steel based on a dispersed phase transformation toughening mechanism. More information on the design and

---

Doc. IIW-2496, recommended for publication by Commission IX “Behaviour of Metals Subjected to Welding”.

X. Yue (✉)  
Welding Engineering Program, The Ohio State University, 1248  
Arthur E. Adams Drive, Columbus, OH 43221, USA  
e-mail: yuexinosu@gmail.com

microstructure development of BA-160 can be referenced in publications by Saha et al. [13, 14].

Because welding is the major fabrication technique used in shipbuilding, it is required that the steels used in hull construction should possess good weldability. Among the weldability issues associated with high-strength steels, heat-affected zone (HAZ) hydrogen-induced cracking (HIC) is perhaps the most serious, and if not well controlled, it can occur unexpectedly and usually lead to catastrophic failure and great loss [15–18]. A number of theories have thus been proposed by researchers over the years to describe the mechanism of HIC, among which some are more popular, such as the surface adsorption theory by Petch [19], the decohesion theory by Troiano [20], and the slip softening model proposed by Beachem [21]. Even though this cracking mechanism has been intensely studied, a unified mechanism does not exist. However, it is generally agreed that the occurrence of HIC require the simultaneous presence of a threshold level of hydrogen, a susceptible microstructure, and tensile residual stress [22].

For the above reasons, the author's PhD research at The Ohio State University focused on investigation of heat-affected zone hydrogen-induced cracking of the new and current high-strength naval steels. The implant test, which was first developed by Henri Granjon at the Institut de Soudure (French Welding Institute) [23], was used to achieve the research goals and proved by researchers to be an very effective testing method [24–27]. This paper is a summary of the author's PhD study, which primarily consists of four parts. Firstly, phase transformation behavior in the CGHAZ of the three steels was studied and continuous cooling transformation diagrams were developed, to better understand the effect of microstructure on HIC susceptibility of the three steels. Secondly, the inherent HIC susceptibility of the three steels was evaluated, and a comparison was made between the performance of the new BA-160 with the currently used HY-100 and HSLA-100. Thirdly, the influence of hydrogen level on the cracking sensitivity of the three steels was studied to understand the steels' tolerance to high hydrogen level without causing cracking in the HAZ. Lastly, the effect of welding parameters on reducing HIC tendency of the new BA-160 was investigated and recommendation was made to reduce HIC when welding BA-160. The research results were employed to develop a weldability database for naval steels, which can be used as a benchmark for developing new high-performance steels in the future.

## 2 Materials and experimental procedures

The base metal microstructures of the three steels are shown in Fig. 1. HY-100 microstructure is quenched and tempered martensite with carbides that form during tempering. HSLA-

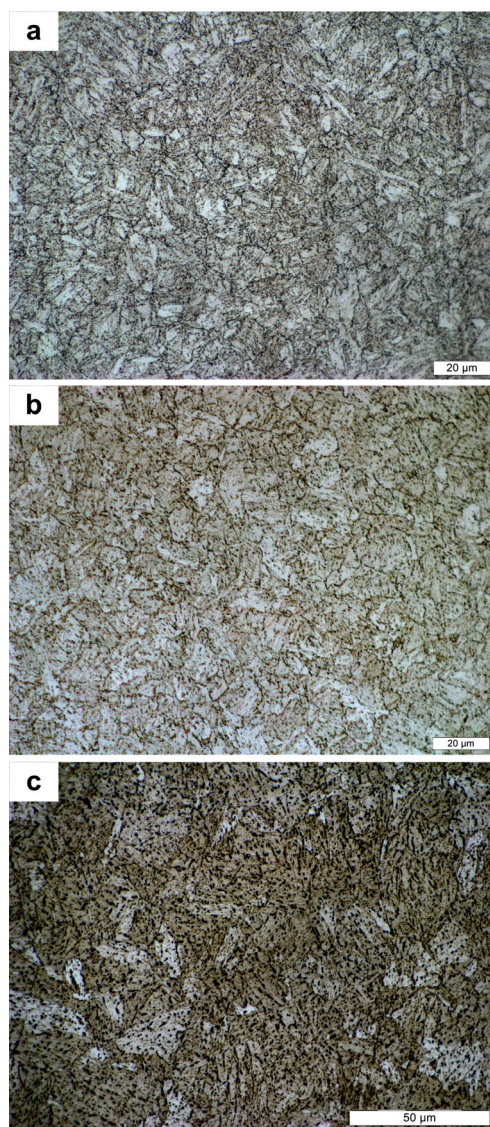


**Fig. 1** Base metal microstructure: **a** HY-100; **b** HSLA-100; **c** BA-160

100 is made by a Thermo-Mechanical Controlled Processing technique. The steel matrix is quenched and tempered martensite and/or bainite with various precipitates providing additional strengthening. BA-160 is a mixture of tempered martensite and bainite, with  $M_2C$  carbides and copper precipitates dispersed in the matrix. Table 1 lists the chemical composition of the three steels.

The CGHAZ simulation for developing the CCT diagrams was performed in a Gleeble 3800<sup>TM</sup>, with experimental details can be found in Ref 28. The implant test was used for the HIC study, as shown in Fig. 2. In the implant test, weld beads were deposited using the gas metal arc welding process with 1.2 mm SuperArc<sup>®</sup> LA-100 wire (AWS: ER100S-G). When comparing the cracking susceptibility of the three steels, heat input was held constant at average 1.3 kJ/mm (33 kJ/in) for all the welding runs (voltage, 30 V; average current, 220 A; travel speed, 5.1 mm/s). Ar+15%H<sub>2</sub> and Ar+

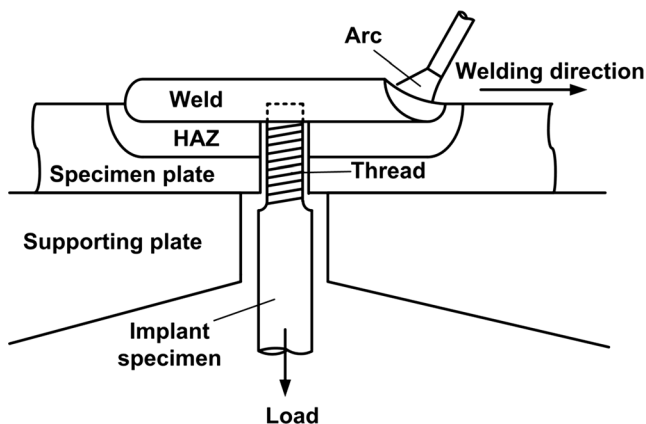
**Table 1** Measured chemical composition of the three steels

Element (wt%)	BA-160	HY-100	HSLA-100
C	0.059	0.18	0.051
Mn	0.001	0.28	0.90
Si	0.015	0.21	0.25
P	<0.005	0.008	0.008
S	<0.001	0.002	0.002
Cu	3.39	0.15	1.17
Ni	6.80	2.32	1.58
Cr	1.90	1.37	0.60
Mo	0.61	0.26	0.37
V	<0.001	<0.01	<0.01
Nb	<0.001	<0.01	0.017
Ti	0.016	<0.01	<0.01

5% $H_2$  shielding gas at a flow rate of 21.2 L/min (45 ft<sup>3</sup>/h) were used in order to introduce a high (10.5 mL/100 g) and a low (6.5 mL/100 g) diffusible hydrogen level into the weld pool, to study the steels' performance under different hydrogen levels. Diffusible hydrogen level was measured using gas chromatograph method in accordance with AWS A4.3.

When evaluating the effect of welding parameters on reducing cracking susceptibility of BA-160, besides the low heat input of 1.3 kJ/mm, a high heat input of 2.6 kJ/mm (66 kJ/in) was also used (voltage, 30 V; average current, 220 A; travel speed, 2.5 mm/s) to evaluate the effect of heat input on the HAZ cracking tendency of BA-160. In addition, for the low heat input of 1.3 kJ/mm, preheat at 60, 100, and 150 °C was applied before welding to evaluate the preheat effect on reducing the HIC tendency. For this part of research, Ar+15% $H_2$  shielding gas at a flow rate of 21.2 L/min was used so the diffusible hydrogen content was kept at 10.5 mL/100 g.

More information on the experimental setup, specimen geometry and the implant testing system (OSU-MITS) etc. can be found in previous publications [29–31].

**Fig. 2** Schematic of the implant test

### 3 Results and discussion

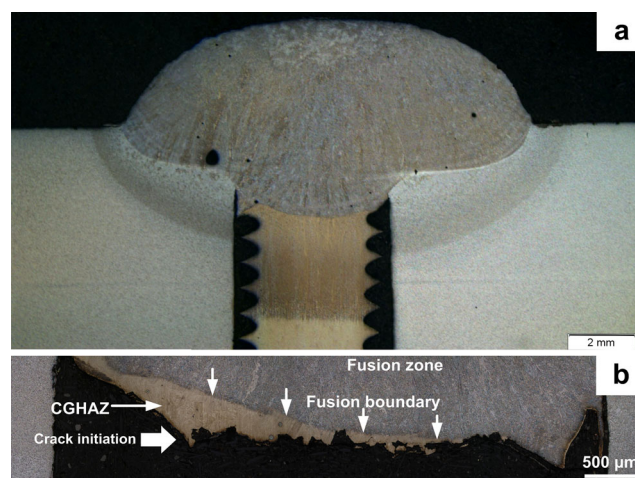
#### 3.1 Weld macrostructure

Figure 3a shows the macrostructure of a typical weld sectioned perpendicular to the welding direction through the axis of the implant specimen. It can be seen that a HAZ was created in the 10–32 UNF thread (per Unified Thread Standard) region of the implant specimen. The diffusible hydrogen was introduced to the weld pool by using the Ar+ $H_2$  mixture shield gas. The hydrogen in the shielding gas decomposed to its atomic state by the follow reaction [32].



Because of the large decrease in solubility when the weld metal solidified, a portion of the atomic hydrogen diffused out of the weld pool due to the reverse of Reaction (1). However, because of the fast cooling rate experienced in welding, some isolated porosities were formed in the fusion zone as a result of insufficient time for hydrogen to escape. Other atomic hydrogen had high diffusivity, diffused down the concentration gradient and penetrated deeper into the fusion boundary and HAZ, which will cause cracking to occur.

The 10-32 UNF thread was machined on the implant specimen to act as a stress concentrator, simulating the stress concentration encountered in the HAZ of real weld joints. Therefore, when the implant specimen was subjected to a static tensile load after welding was completed, cracking occurred in the stress concentrated HAZ regions instead of the fusion zone, and it happened in the most HIC susceptible HAZ region. It has been shown that the coarse-grained HAZ (CGHAZ) is the region where crack initiates and propagates, as a result of the coarse prior austenite grain size as well as the formation of susceptible microstructure with high hardness

**Fig. 3** a Representative weld macrostructure; b macrostructure of a typical fractured joint after loading showing the fracture path



[33–35]. Figure 3b shows a typical cracking propagation path, in which it can be seen that the hydrogen crack initiates from the root of the first unfused thread closest to the fusion boundary, indicated by the four parallel white arrows, and propagates in the CGHAZ approximately 0.1–0.3 mm away from the fusion boundary. Since CGHAZ is the most HIC susceptible region in the entire HAZ, phase transformation behavior in the CGHAZ was studied, which will be discussed in the next section.

### 3.2 Continuous cooling transformation diagrams of the CGHAZ of the three steels

It was found that CGHAZ is the most susceptible to HIC in the HAZ regions. Therefore, the continuous cooling transformation (CCT) diagrams for the CGHAZ of the three steels were developed to better understand the phase transformation behavior in the CGHAZ, as shown in Fig. 4. Detailed information can be referenced in previous publications [10, 28].

As a result of the difference of the steels' chemical composition, the three steels have different hardenability indicated by the carbon equivalent. Different phase transformation products form in the three steels' CGHAZ. It can be seen that both bainite and martensite form in the CGHAZ of HY-100 and HSLA-100, and HY-100 has a higher hardenability than HSLA-100. While for BA-160, martensite was found to be the predominant phase in the CGHAZ, suggesting BA-160 has the highest hardenability among the three steels.

### 3.3 Vickers hardness test results

Vickers hardness measurements were performed on the weld joints along the axis of the implant specimens. It was started in the fusion zone, and ran through the HAZ to the unaffected base metal of the implant specimens, to illustrate the hardness variation in different regions. The hardness traverse for the three steels are shown in Fig. 5.

As shown in Fig. 5, the data within the two black solid lines represent the hardness of the HAZ of the implant specimens. Because CGHAZ is the most HIC susceptible region, it is indicated in the hardness traverse by drawing a red dotted line as the approximate boundary separating CGHAZ and its adjacent fine-grained HAZ.

It can be seen in Fig. 5a that for HY-100 with 1.3 kJ/mm heat input, a hardness plateau is present across the whole HAZ region. The CGHAZ hardness is in the range of 440–464 HV<sub>1.0</sub>, which is much higher than the fusion zone and HY-100 base metal. While for HSLA-100 with 1.3 kJ/mm heat input, the CGHAZ hardness is in the range of 293–329 HV<sub>1.0</sub>, which is slightly higher than the fusion zone and HSLA-100 base metal and the lowest among the three steels'

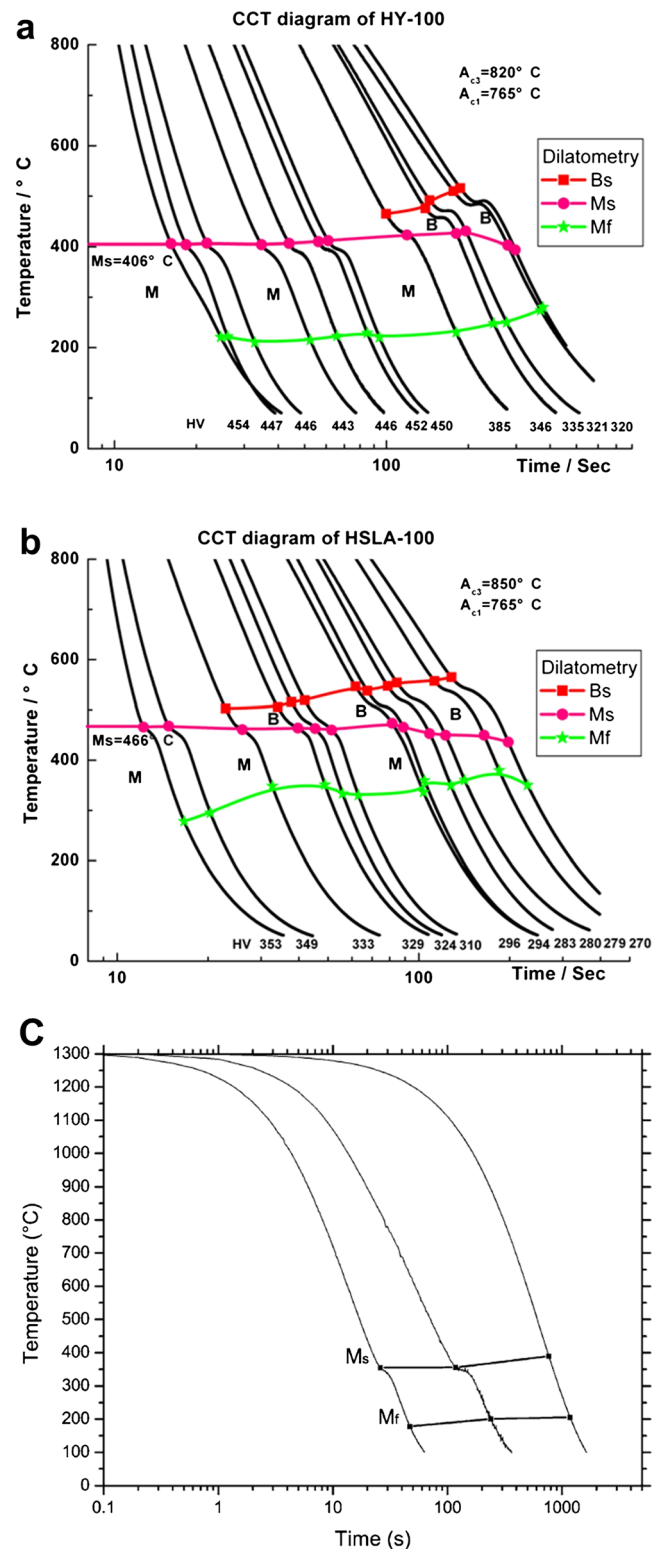
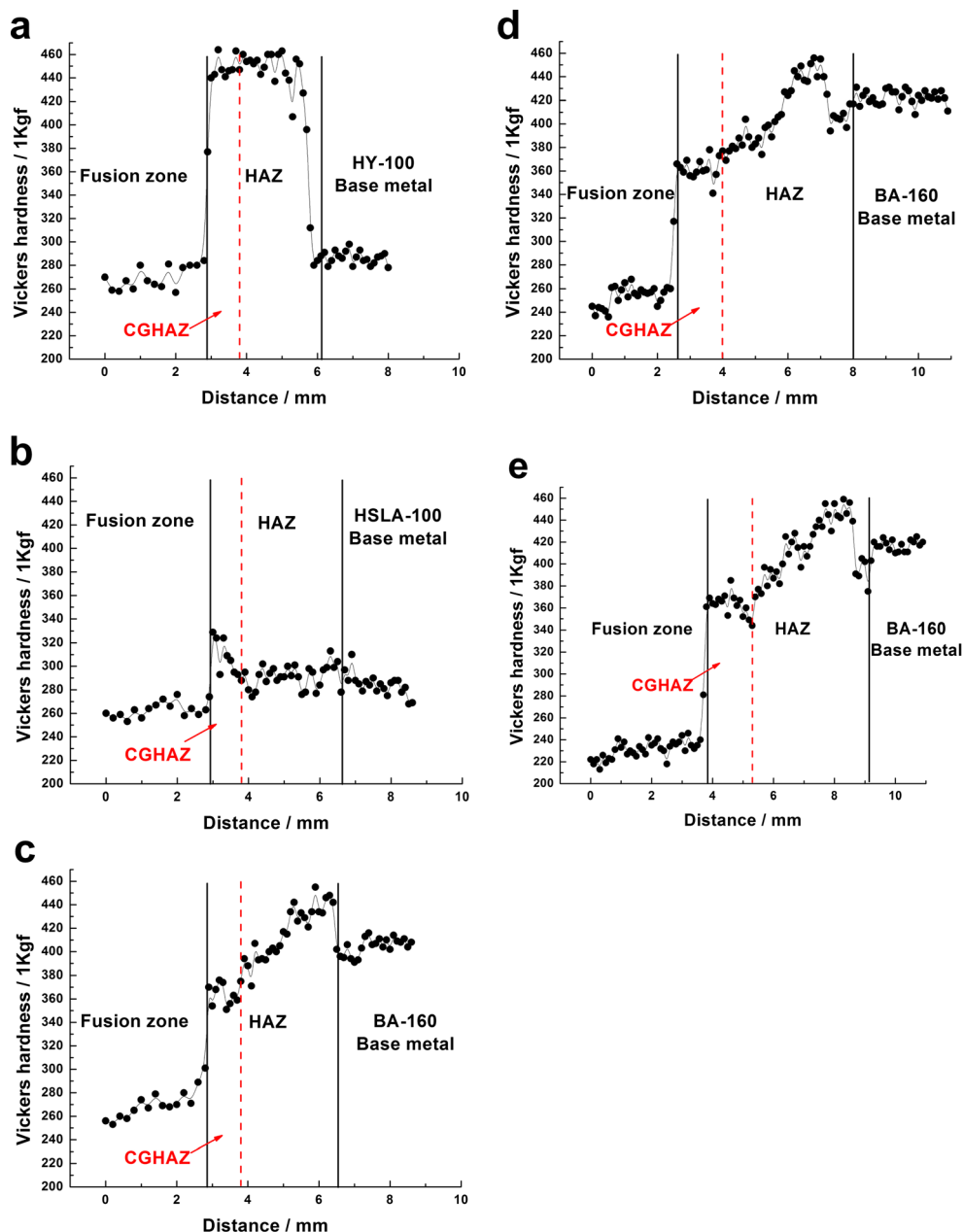


**Fig. 4** Continuous cooling transformation diagrams for the CGHAZ of the three steels. **a** HY-100; **b** HSLA-100; **c** BA-160 (reprinted from Ref. [10])

CGHAZ. In addition, the prior austenite grain size for HSLA-100 is around 50  $\mu\text{m}$ , which is also the smallest among the three steels.

**Fig. 5** Vickers hardness measurements taken along the axis of the implant specimens. **a** HY-100, 1.3 kJ/mm heat input; **b** HSLA-100, 1.3 kJ/mm heat input; **c** BA-160, 1.3 kJ/mm heat input; **d** BA-160, 2.6 kJ/mm heat input; **e** BA-160, 1.3 kJ/mm heat input with preheat at 150 °C before welding



For BA-160, as shown in Fig. 5c–e, it can be seen that the hardness increases gradually from the CGHAZ to the FGHAZ and into the intercritical HAZ (ICHAZ). The hardness of CGHAZ is in the range of 350–376 HV<sub>1.0</sub> with 1.3 kJ/mm heat input, which is the lowest among the HAZ regions and even lower than that of the BA-160 base metal, resulting in a “softening” in the HAZ. This phenomenon was explained based on the relative strength contributions from lath martensite morphology and Cu precipitates in different HAZ regions [12]. Further research found that strength of this softening region can be recovered using an appropriate postweld heat treatment (PWHT) [36]. Even though the CGHAZ hardness is lower than other HAZ

regions, it was found this is the most HIC susceptible region, where the crack initiation and propagation occur, as shown in the previous section. That is because the detrimental grain coarsening dominates over the hardness impact, and it was observed that the prior austenite grain size of HY-100 and BA-160 CGHAZ is in the range of 70–80 μm [10, 28].

When welding BA-160 with 2.6 kJ/mm heat input or welding with 1.3 kJ/mm heat input combined with preheat at 150 °C, as shown in Fig. 5d, e, the average CGHAZ hardness is 358 and 363 HV<sub>1.0</sub>, respectively, which are slightly lower than 370 HV<sub>1.0</sub> of welding with 1.3 kJ/mm heat input. This is because using higher heat input and/or using preheat results in

slower cooling rate, which may result in the formation of lower-hardness phases in the CGHAZ.

### 3.4 Microstructure characterization of CGHAZ of the three steels

Microstructure dictates the HIC susceptibility of a steel, therefore the microstructure of CGHAZ is one of the most important variables to control the HIC susceptibility of a weld joint since CGHAZ is the weakest link. Generally speaking, microstructure with a higher hardness is more susceptible to HIC compared with lower-hardness microstructure. Martensite in any form is more susceptible to HIC than higher-temperature austenite decomposition products such as ferrite, pearlite and bainite. And for martensite, twinned martensite with higher carbon content is more susceptible to HIC than low-carbon lath martensite.

The CGHAZ microstructure of the three steels welded with 1.3 kJ/mm heat input has been characterized by means of optical microscopy and transmission electron microscopy (TEM), as shown in Figs. 6, 7, and 8. Under a specific cooling rate, the steel's composition, dictating the hardenability, determines the on-cooling phase transformation behavior of the CGHAZ. Carbon is recognized as the strongest element to increase hardenability, and other alloying elements such as Cr, Mo, Ni, and Cu also have strong influence. Both BA-160 and HY-100 have significant alloying addition, and their carbon

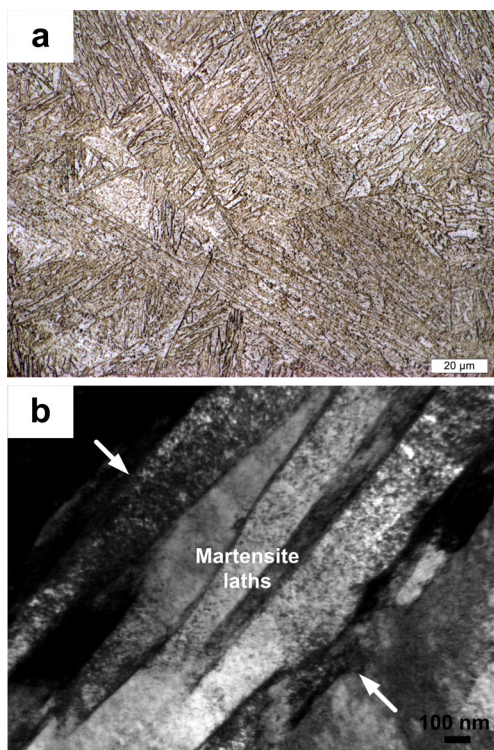


**Fig. 6** CGHAZ microstructure of BA-160, 1.3 kJ/mm heat input. **a** Optical; **b** bright-field TEM

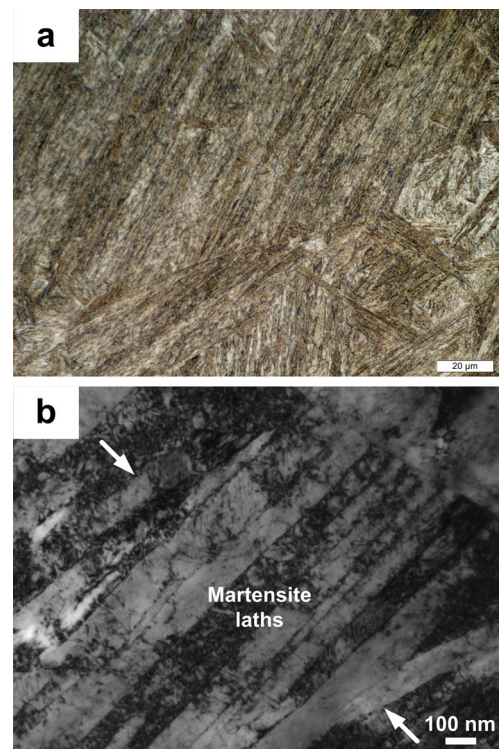


**Fig. 7** CGHAZ microstructure of HY-100, 1.3 kJ/mm heat input. **a** Optical; **b** bright-field TEM

equivalent is calculated to be 1.24 and 0.75, respectively. The high alloying addition and corresponding high hardenability of the two steels result in the formation of predominant martensite in the CGHAZ microstructure, which is the dark-etching phase as shown in Figs. 6a and 7a, and no ferrite and/or bainite can be observed in the microstructure. The martensite laths can be resolved at the respective high-magnification TEM bright-field pictures, as shown in Figs. 6b and 7b. The formation of lath martensite instead of twinned martensite in the microstructure is because of the low carbon addition in the two steels, which is 0.059 wt% for BA-160 and 0.18 wt% for HY-100.

The CGHAZ microstructure of HSLA-100 is shown in Fig. 8. The microstructure is a mixture of martensite and bainite. It is shown in Fig. 8a that bainite is the light-etching needle-like phase and martensite is the dark-etching phase. The TEM picture, as shown in Fig. 8b, is used to further distinguish bainite and martensite in the microstructure. A group of parallel laths free of precipitates is observed in the lower-left part of Fig. 8b, which are martensite laths. While in the upper-right corner of Fig. 8b, intralath platelet-like cementite precipitates can be seen, which are oriented at approximately 55° from the primary lath growth direction, and this is the distinguishing feature of lower bainite from upper bainite and martensite [37]. The formation of bainite in the microstructure results in a lower CGHAZ hardness than BA-160 and HY-100, which is in the range of 293–329 HV<sub>1.0</sub>.



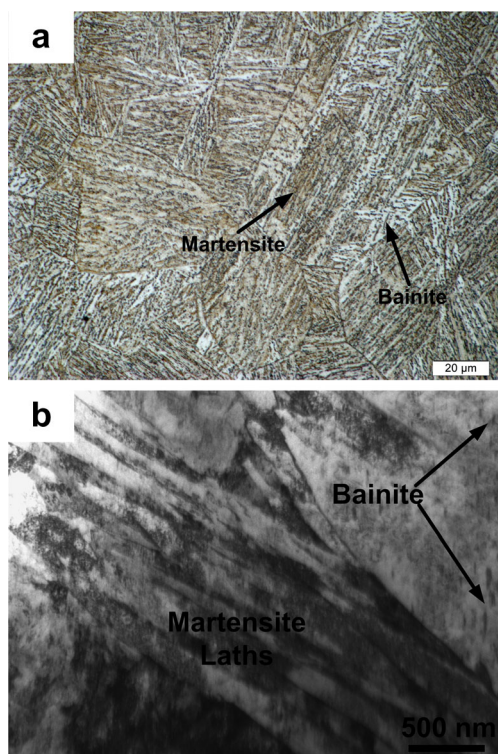


**Fig. 8** CGHAZ microstructure of HSLA-100, 1.3 kJ/mm heat input. **a** Optical; **b** bright-field TEM

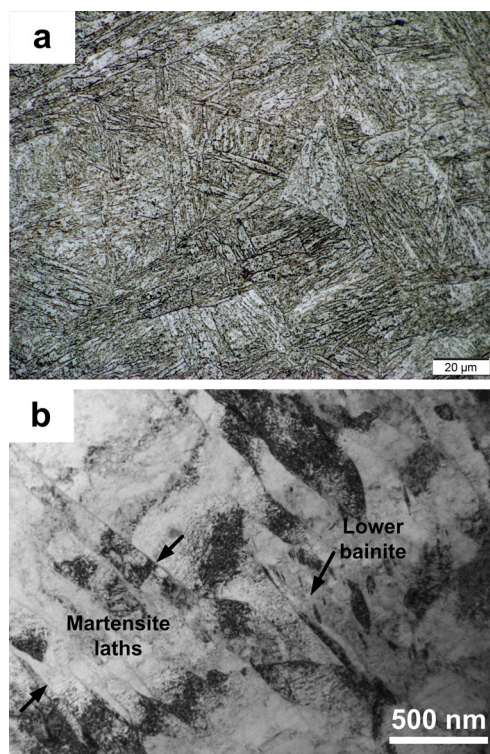


**Fig. 9** CGHAZ microstructure of BA-160, 2.6 kJ/mm heat input. **a** Optical; **b** bright-field TEM

When welding BA-160 with 2.6 kJ/mm heat input, it is found that martensite is the predominant phase in the microstructure as shown in Fig. 9a. However, the TEM picture (Fig. 9b) shows the formation of lower bainite in the CGHAZ. Note that lower bainite may only represent a small fraction of the CGHAZ microstructure, and because of the thin laths and limited amount, it cannot be resolved in the optical microscope. The formation of lower bainite in the CGHAZ therefore decreases the average CGHAZ hardness to 358 HV<sub>1.0</sub> compared with the martensitic microstructure in CGHAZ with 1.3 kJ/mm heat input of an average hardness of 370 HV<sub>1.0</sub>. It is shown in Fig. 10 that when welding with 1.3 kJ/mm heat input and preheat at 150 °C, the CGHAZ microstructure still consists of predominant martensite. Similarly, as the average hardness of 363 HV<sub>1.0</sub> is lower than that welded without preheat, it is postulated that a small quantity of lower-hardness bainite may form in the CGHAZ because of the lower cooling rate by preheating.

### 3.5 Comparison of the three steels with respect to hydrogen cracking susceptibility

The implant test results for the three steels welded with Ar+5%H<sub>2</sub> and Ar+15%H<sub>2</sub> shielding gas are shown in Figs. 11 and 12. Application of the two shielding gas introduced a low (6.5 mL/100 g) and a high (10.5 mL/100 g) level of diffusible hydrogen into the weld pool. Therefore, the sensitivity of the

three steels to different hydrogen levels in the weld pool can be evaluated. Determining the susceptibility to HIC as a

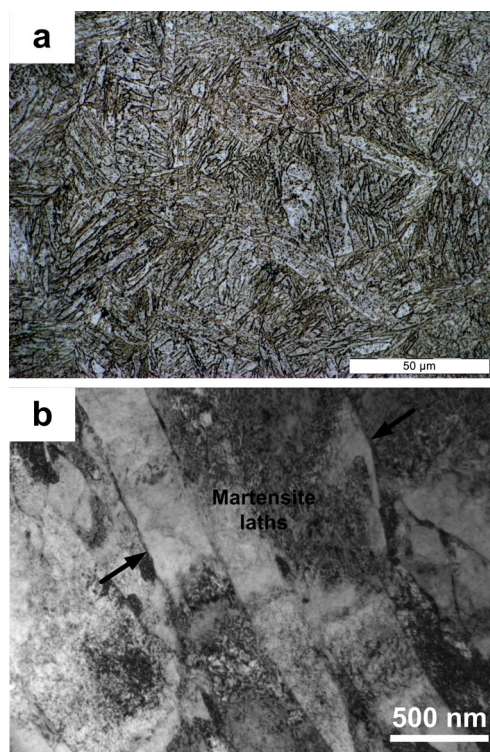


**Fig. 10** CGHAZ microstructure of BA-160, 1.3 kJ/mm heat input and preheat at 150 °C before welding. **a** Optical; **b** bright-field TEM

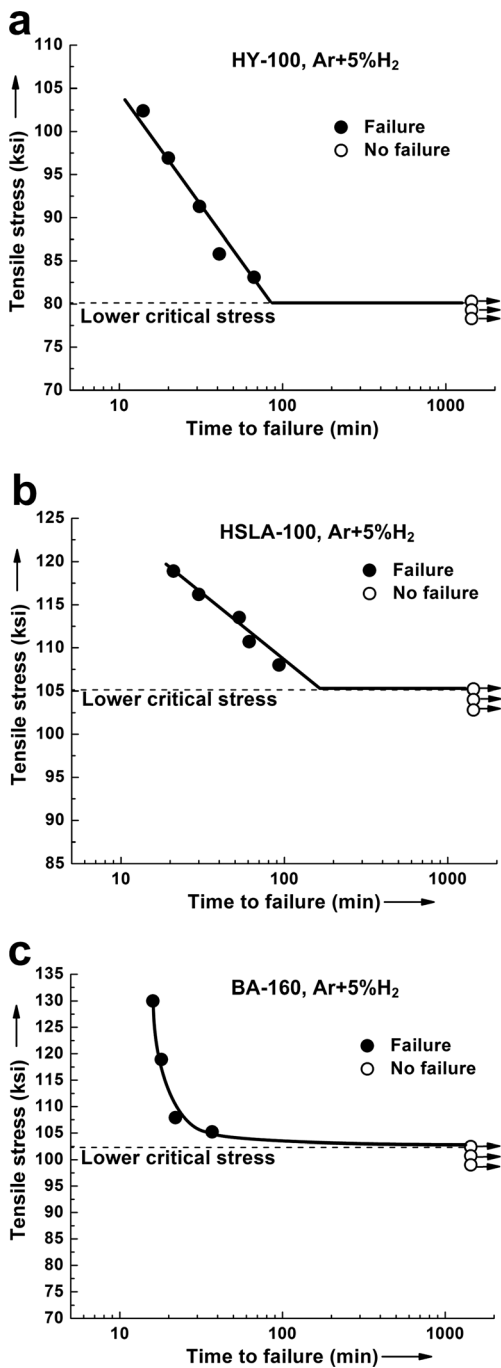


**Fig. 11** The implant test curves of: **a** HY-100; **b** HSLA-100; **c** BA-160. Welded with Ar+5%H<sub>2</sub> shielding gas and 1.3 kJ/mm heat input

function of hydrogen level is of critical importance. That is because high-strength steels having a good tolerance to higher hydrogen level without cracking are desired from a practical welding standpoint since the welding requirements (preheat, interpass, and postweld heat treatment controls) can be relaxed.

For HY-100, when the diffusible hydrogen level is low, 6.5 mL/100 g, the lower critical stress (LCS) was determined to be 80 ksi (551 MPa). However, when the high hydrogen

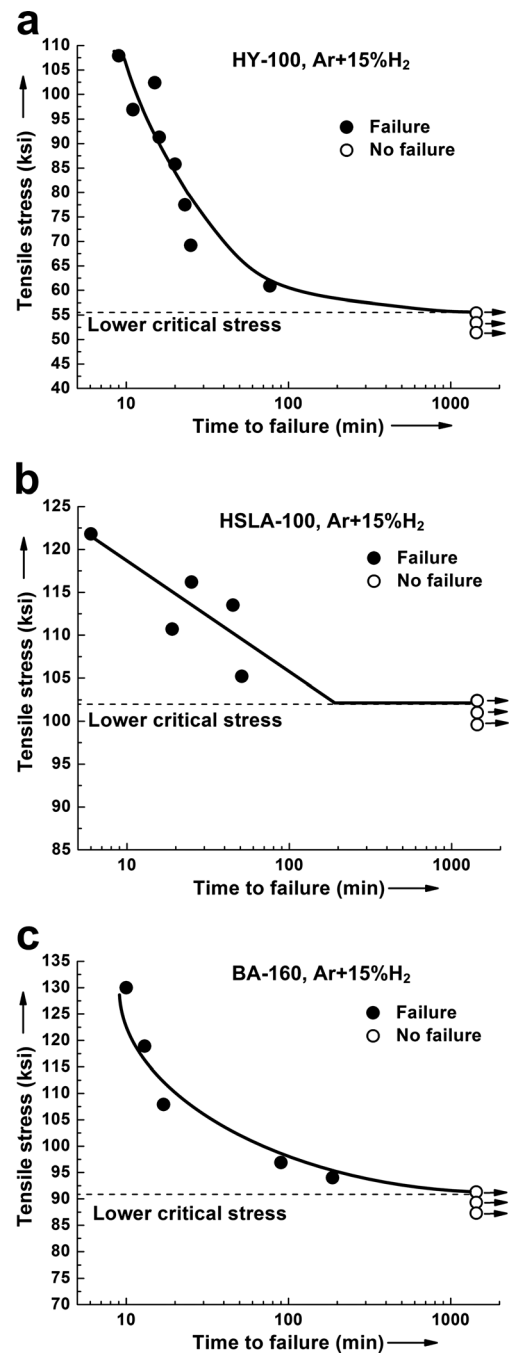


**Fig. 12** The implant test curves of: **a** HY-100; **b** HSLA-100; **c** BA-160. Welded with Ar+15%H<sub>2</sub> and 1.3 kJ/mm heat input

level of 10.5 mL/100 g was introduced, the LCS was drastically decreased to 55 ksi (379 MPa). For HSLA-100, the LCS decreased from 105 ksi (723 MPa) when welding with high hydrogen to 102 ksi (703 MPa) when welding with low hydrogen.

For BA-160, with the low diffusible hydrogen level, the LCS was determined to be 102 ksi (703 MPa). And it decreased to 91 ksi (627 MPa) with the high diffusible hydrogen level. The LCS decrease for BA-160 is 11 ksi (76 MPa) with



increasing diffusible hydrogen content, which is less than that of 25 ksi (172 MPa) for HY-100 but more than that of 3 ksi (20 MPa) for HSLA-100. This indicates that BA-160 has a better tolerance to more diffusible hydrogen without a significant reduction in HIC resistance than HY-100, but is more sensitive to hydrogen content in the weld joint compared with HSLA-100.

Besides the comparison of the performance of the three steels under different diffusible hydrogen levels, the other comparison, which is about the inherent susceptibility to HIC, has been made based on the implant test results, as summarized in Table 2. Because the three steels have different grades of yield strength, the LCS should be “normalized” then can be used for the comparison [38]. An Embrittlement Index (EI) was proposed and used in the present study to compare the three steels. EI is defined as the ratio of LCS to the CGHAZ tensile strength of the test steel. However, as it is difficult to measure the CGHAZ tensile strength directly from the implant test, an acceptable approximation can be obtained by converting from the maximum CGHAZ hardness value according to the ASTM hardness conversion chart. The higher the EI, the lower the CGHAZ susceptibility to HIC. Using the implant test results under the two diffusible hydrogen levels, the EI of BA-160 is determined to be 0.59 (low hydrogen) and 0.53 (high hydrogen), which is higher than the corresponding EI value of 0.36 (low hydrogen) and 0.24 (high hydrogen) for HY-100, but lower than that of 0.7 (low hydrogen) and 0.68 (high hydrogen) for HSLA-100. This suggests that BA-160 has a better inherent resistance to HIC than HY-100, though its carbon equivalent is higher than that of HY-100. However, BA-160 is more inherently susceptible to HIC compared with HSLA-100.

### 3.6 Effect of welding parameters on reducing hydrogen cracking susceptibility of BA-160

In order for the new steel BA-160 to be welded with good resistance to HAZ HIC, an understanding of the effect of welding parameters on reducing the cracking tendency is required. Therefore, the implant test was also used in the

present study to evaluate the HAZ HIC tendency of BA-160 under different welding conditions (varying heat input and preheat), with the test results summarized in Table 3.

Heat input is a factor that affects the HIC tendency. Varying heat input will change the cooling rate and lead to the formation of different microstructures in the CGHAZ during cooling after welding. As discussed in the previous section, the low heat input of 1.3 kJ/mm results in a harder BA-160 CGHAZ microstructure as compared to that welded with the high heat input of 2.6 kJ/mm.

The implant test results for welding BA-160 with different welding parameters using Ar+15% $H_2$  shielding gas are shown in Fig. 13. The LCS values were determined to be 91 ksi (627 MPa) and 96 ksi (661 MPa) for low and high heat input, respectively. The increase in LCS when using high heat input indicates that increasing heat input when welding BA-160 steel reduces the tendency for HIC in the CGHAZ. The reduction in cracking susceptibility when using high heat input can also be seen by the comparison of the incubation time before failure. When the applied stress is 107 ksi (737 MPa), the incubation time for the low heat input is 17 min, while it increases to 139 min for the high heat input.

Clearly, the reduced HIC susceptibility for the CGHAZ of BA-160 when increasing heat input is because of formation of different microstructure as a result of slower cooling rates. The lower-hardness microstructure of the mixed martensite and lower bainite formed at slow cooling rate has a better resistance to cracking as compared to the higher hardness martensitic microstructure formed at low heat input.

However, it should be noted that in real welding practice, reducing HAZ HIC tendency by using a very high heat input may either not be practical or lead to severe grain coarsening, which may either reduce toughness or cause softening. As a result, the determination of heat input should also consider other factors.

The implant test was also carried out with low heat input and preheat temperatures of 60, 100, and 150 °C to evaluate the preheat effect on reducing the cracking tendency, as shown in Fig. 13b–d. It can be seen that with preheat before welding, all three curves show that the incubation time prior to failure is

**Table 2** Implant test results of three steels welded with 1.3 kJ/mm heat input

Steel	CGHAZ max hardness (HV)	CGHAZ tensile strength <sup>a</sup> ksi (MPa)	Lower critical stress ksi (MPa)		Embrittlement Index <sup>b</sup>		$CE_{AWS}$ <sup>c</sup>
			Low hydrogen	High hydrogen	Low hydrogen	High hydrogen	
HY-100	464	225 (1,550)	80 (551)	55 (379)	0.36	0.24	0.75
HSLA-100	329	150 (1,034)	105 (723)	102 (703)	0.7	0.68	0.62
BA-160	376	173 (1,192)	102 (703)	91 (627)	0.59	0.53	1.24

<sup>a</sup> The CGHAZ tensile strength is converted from the CGHAZ max hardness using the ASTM hardness conversion chart

<sup>b</sup> Embrittlement Index is the ratio of lower critical stress to the CGHAZ tensile strength

<sup>c</sup> AWS carbon equivalent:  $CE_{AWS} = C + (Mn + Si)/6 + (Cr + Mo + V)/5 + (Ni + Cu)/15$

**Table 3** Summary of microstructure, hardness and implant test results for different welding conditions for BA-160 welded with Ar+15% $H_2$ 

Welding conditions	Low HI (1.3 kJ/mm)	High HI (2.6 kJ/mm)	Low HI (1.3 kJ/mm), preheat at 60 °C	Low HI (1.3 kJ/mm), preheat at 100 °C	Low HI (1.3 kJ/mm), preheat at 150 °C
CGHAZ microstructure	M	M+B	M	M	M+(B) <sup>a</sup>
CGHAZ Hardness (Avg) <sup>b</sup>	370	358	368	366	363
Implant test LCS	91 ksi (627 MPa)	96 ksi (661 MPa)	94 ksi (648 MPa)	103 ksi (710 MPa)	107 ksi (737 MPa)

<sup>a</sup> *M* represents martensite; *B* represents bainite; (*B*) represents possible formation of bainite in the microstructure

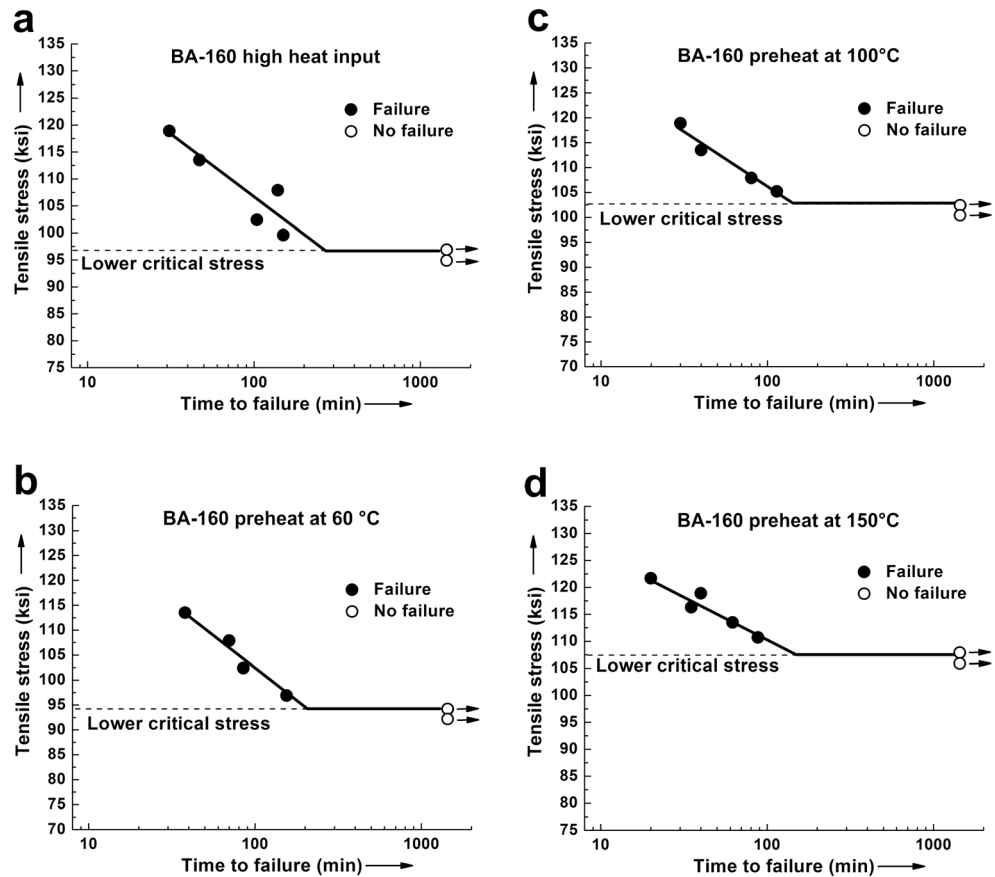
<sup>b</sup> *Avg* means the average hardness of the CGHAZ, which is determined by taking the average of hardness data points in the CGHAZ region together. The approximate boundary of CGHAZ is determined by metallographic observation

longer than that without preheat at equivalent tensile stress levels, as compared to Fig. 12c, indicating applying preheat reduces HAZ cracking tendency. This is possibly because applying preheat can reduce the diffusible hydrogen content, and thereby a longer incubation time is required to reach the critical hydrogen level to cause cracking to occur.

The LCS with preheating at 60 °C was determined to be 94 ksi (648 MPa), which is slightly higher than 91 ksi (627 MPa) without preheat. Increasing the preheat temperature to 100 °C, the LCS was increased to 103 ksi (710 MPa), and this was also with a concomitant increase in incubation time. By further increasing the preheat temperature to 150 °C, the LCS was increased to 107 ksi (737 MPa). This clearly

indicates that increasing preheat temperature is beneficial to reduce HAZ cracking tendency for BA-160. However, increasing preheat temperature to 150 °C to reduce cracking was not so effective compared with the 9 ksi LCS increase from preheat at 60 °C to at 100 °C. Based on the implant test results, it is shown that applying preheat and increasing preheat temperature are beneficial to reduce the cracking tendency for BA-160. One reason is that applying preheat results in a slower cooling rate, which leads to the formation of a lower-hardness microstructure in the CGHAZ as found in the Vickers hardness test results. The other reason is that preheat may be effective to reduce the diffusible hydrogen level in the HAZ as discussed previously.

**Fig. 13** The implant test curves for welding BA-160 with different welding parameters using Ar+15% $H_2$ . **a** 2.6 kJ/mm heat input; **b** 1.3 kJ/mm heat input and preheat at 60 °C; **c** 1.3 kJ/mm heat input and preheat at 100 °C; **d** 1.3 kJ/mm heat input and preheat at 150 °C



### 3.7 Fracture behavior

Since fractography is a good indication of steels' susceptibility to HIC, the fracture surface of failed implant specimens of the three steels were studied under SEM. Representative SEM fractographs are presented in Fig. 14. It shows that the fracture surface can be divided into different regions based on morphology. In Fig. 14a, the white arrow indicates the crack propagation direction.

It is found that coarse intergranular (IG) (Fig. 14b) is the dominant fracture mode in the crack initiation region. As the crack propagates, quasi-cleavage (QC) (Fig. 14c) and microvoid coalescence (MVC) (Fig. 14d) fracture modes are observed in sequence along the crack propagation direction.

The sequential occurrence of IG, QC and MVC fracture modes on implant specimen fracture surface was explained using Beachem's model [21], as shown in Fig. 15. Assume when the implant specimen is subjected to loading after welding, the combination of stress intensity factor and hydrogen concentration at the crack tip corresponds to point a in Fig. 15. The hydrogen concentration is not sufficient to initiate a crack, so cracking will not occur immediately. During the incubation period, atomic hydrogen continuously diffuses to the triaxially stressed region and after some time, it will reach the critical level indicated by point b in Fig. 15. A crack is then initiated in the CGHAZ and grow intergranularly. As the crack propagates, the stress intensity factor increases while the hydrogen level decreases to point c, promoting a QC fracture mode. As the crack continues to grow, and if the combination of stress intensity factor and hydrogen

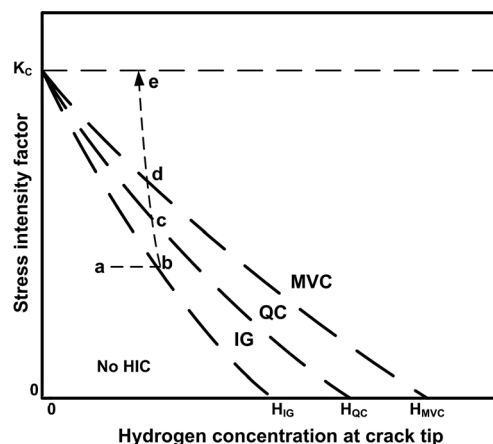


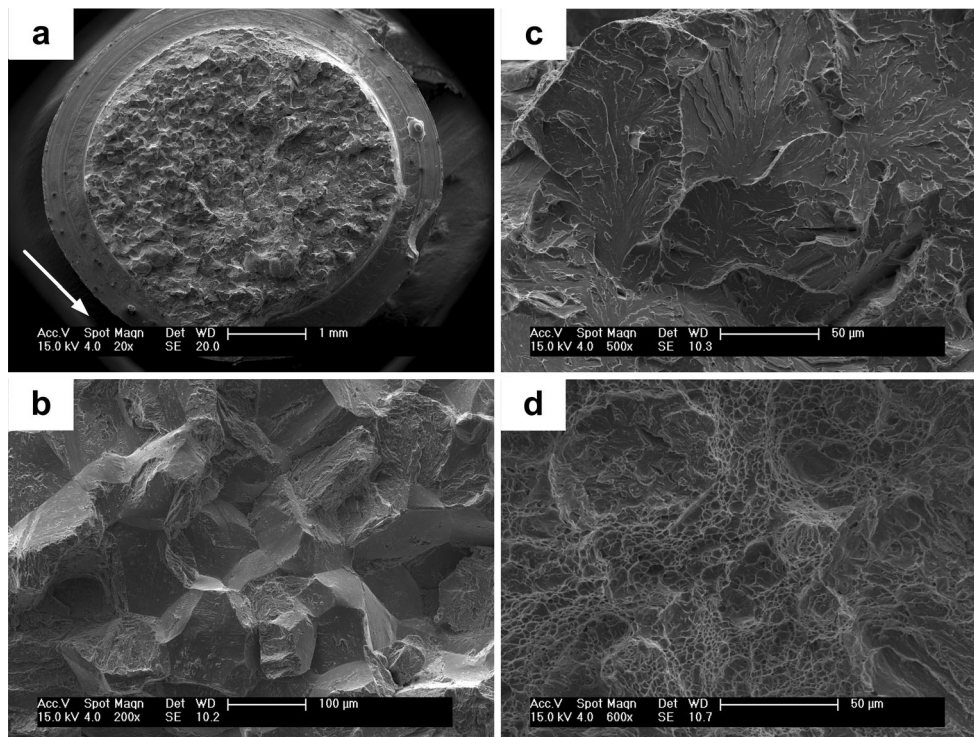
**Fig. 15** Combined effect of stress intensity factor and hydrogen concentration at crack tip on the fracture mode

concentration reaches point d, the fracture mode changes to MVC. If the stress intensity factor continues to increase to the critical value  $K_C$ , ultimate failure take place.

When comparing the fracture surface of BA-160, HY-100, and HSLA-100, it was found that no large area of IG failure can be observed on the fracture surface of BA-160. Among the three steels, the largest area of IG failure with the coarsest grains was found on the fracture surface of HY-100. Since IG involves the least amount of plastic deformation compared to QC and MVC modes, presence of a large area of IG on the fracture surface generally indicates a high potential for HIC.

When welding BA-160 with different parameters, it was found that both using the high heat input and applying preheat

**Fig. 14** Fracture morphology of a failed implant specimen after loading, HY-100. **a** General fracture appearance (white arrow indicates the direction of crack growth); **b** coarse intergranular; **c** quasi-cleavage; **d** microvoid coalescence. **b**, **c**, and **d** are observed in sequence along the crack propagation path





eliminate the IG fracture mode, and increase the MVC area on the fracture surface as compared to the low heat input condition. This is another indication that increasing heat input and/or using preheat improve HIC resistance of BA-160. More information on the fractography study can be found in previous publications [29–31].

#### 4 Conclusions

1. It was found that CGHAZ is the most susceptible to HIC in the entire HAZ. Phase transformation behavior in the CGHAZ of BA-160, HY-100 and HSLA-100 was studied and the continuous cooling transformation diagrams were developed.
2. It is shown in the CCT diagrams that both bainite and martensite form in the CGHAZ of HY-100 and HSLA-100 depending on the cooling rate. While for BA-160, martensite was found to be the predominant phase in the CGHAZ. With respect to hardenability, from the highest to the lowest, is BA-160, HY-100, and HSLA-100.
3. The implant test results with a low and a high hydrogen level show that BA-160 has a better tolerance to more diffusible hydrogen without a significant reduction in HIC resistance than HY-100, but is more sensitive to high hydrogen level in the weld joint compared with HSLA-100.
4. Comparing the three steels, it can be concluded that BA-160 has a better inherent resistance to HIC than HY-100, though its carbon equivalent is higher than that of HY-100. However, BA-160 is more inherently susceptible to HIC compared with HSLA-100. The difference in HIC resistance of CGHAZ is a result of formation of different microstructures.
5. It is shown that both using a high heat input and applying preheat are beneficial to reduce the cracking tendency for BA-160. Firstly, it is because lower-hardness microstructure forms in the CGHAZ when using high heat input and/or using preheat. In addition, using preheat may be effective to reduce the diffusible hydrogen level in the HAZ.
6. IG, QC and MVC fracture modes are observed in sequence along the crack propagation direction on the implant specimen fracture surface. This phenomenon was successfully explained using the Beachem's model. Fractography is a good indication of steels' susceptibility to HIC. Using high heat input and/or preheat eliminate the IG fracture mode, and increase the MVC area on the fracture surface, supporting the implant test results.

**Acknowledgments** The author gratefully acknowledges the financial support of the Office of Naval Research, Award No. N000140811000. Grant Officers: Dr. Julie Christodoulou and Dr. William Mullins. The

author would like to thank Johnnie DeLoach, Matthew Sinfield, and Jeffrey Farren with the Naval Surface Warfare Center Carderock Division, West Bethesda, MD for providing the naval steels used in this study. Thanks are extended to Prof Gregory Olson's research group in Northwestern University for collaboration on this research project and QuesTek Innovations LLC for providing the BA-160 steel. Dejian Liu and Geoffrey Taber are acknowledged for their constructive ideas and assistance with building the implant testing system.

#### References

1. Montemarano TW, Sack BP, Gudas JP, Vassilaros MG, Vanderveldt HH (1986) High strength low alloy steels in naval construction. *J Ship Prod* 2(3):145–162
2. Czyryca EJ (1993) Advances in high strength steel technology for naval hull construction. *Key Eng Mater* 84–85:491–520
3. Vassilaros MG, Czyryca EJ (1993) The development of high-strength, cooling-rate insensitive ultra-low-carbon steel weld metals. *Key Eng Mater* 84–85:587–601
4. Czyryca EJ, Link RE, Wong RJ, Aylor DA, Montemarano TW, Gudas JP (1990) Development and certification of HSLA-100 steel for naval ship construction. *Nav Eng J* 102(3):63–82
5. Isheim D, Gagliano MS, Fine ME, Seidman DN (2006) Interfacial segregation at Cu-rich precipitates in a high-strength low-carbon steel studied on a sub-nanometer scale. *Acta Mater* 54:841–849
6. Kolli RP, Seidman DN (2008) The temporal evolution of the decomposition of a concentrated multicomponent Fe-Cu-based steel. *Acta Mater* 56:2073–2088
7. Vaynman S, Isheim D, Kolli RP, Bhat SP, Seidman DN, Fine ME (2008) High-strength low-carbon ferritic steel containing Cu-Fe-Ni-Al-Mn precipitates. *Metall Mater Trans A* 39:363–373
8. Hunter AH, Farren JD, Dupont JN, Seidman DN (2013) An atom-probe tomographic study of arc welds in a multi-component high strength low alloy steels. *Metall Mater Trans A* 44:1741–1759
9. Farren JD, Hunter AH, Dupont JN, Seidman DN, Robino CV, Kozeschnik E (2012) Microstructural evolution and mechanical properties of fusion welds in an iron-copper-based multicomponent steel. *Metall Mater Trans A* 43:4155–4170
10. Caron JL, Babu SS, Lippold JC (2011) Welding-induced microstructure evolution of a Cu-bearing high-strength blast-resistant steel. *Metall Mater Trans A* 42:4015–4031
11. Caron JL, Babu SS, Lippold JC (2011) Weldability evaluation of a Cu-bearing high-strength blast-resistant steel. *Metall Mater Trans A* 42:4032–4044
12. Yu X, Caron JL, Babu SS, Lippold JC, Isheim D, Seidman DN (2010) Characterization of microstructural strengthening in the heat-affected zone of a blast-resistant naval steel. *Acta Mater* 58:5596–5609
13. Saha A, Olson GB (2007) Computer-aided design of transformation toughened blast resistant naval hull steels: part I. *J Comput Aided Mater Des* 14:177–200
14. Saha A, Jung J, Olson GB (2007) Prototype evaluation of transformation toughened blast resistant naval hull steels: part II. *J Comput Aided Mater Des* 14:201–233
15. Devletian JH, Fichtelberg ND (2001) Controlling hydrogen cracking in shipbuilding. *Weld J* 80(11):46–52
16. Rowe MD, Nelson TW, Lippold JC (1999) Hydrogen-induced cracking along the fusion boundary of dissimilar metal welds. *Weld J* 78(2):31s–37s
17. Alexandrov B, Theis K, Streitenberger M, Herold H, Martinek I (2005) Cold cracking in weldments of steel S 690 QT. *Weld World* 49:64–73
18. Yurioka N, Suzuki H (1990) Hydrogen assisted cracking in C-Mn and low alloy steel weldments. *Int Mater Rev* 35(4):217–249

19. Petch NJ, Stables P (1952) Delayed fracture of metals under static load. *Nature* 169(4307):842–843
20. Troiano AR (1960) The role of hydrogen and other interstitials in the mechanical behavior of metals. *Trans ASM* 52:54–80
21. Beachem CD (1972) A new model for hydrogen-assisted cracking (hydrogen “embrittlement”). *Metall Trans* 3:437–451
22. Kou S (2003) *Welding metallurgy*. Wiley, New Jersey, pp 410–417
23. Granjon H (1969) The implants method for studying the weldability of high strength steels. *Met Constr Br Weld J* 1(11):509–515
24. Kannengiesser T, Boellinghaus T (2013) Cold cracking tests—an overview of present technologies and applications. *Weld World* 57(1):3–37
25. Sawhill JM, Dix AW, Savage WF (1974) Modified implant test for studying delayed cracking. *Weld J* 53(12):554s–560s
26. Signes EG, Howe P (1988) Hydrogen-assisted cracking in high-strength pipeline steels. *Weld J* 67(8):163s–170s
27. Mayudeeswaran G, Balasubramanian V, Reddy GM (2008) Hydrogen induced cold cracking studies on armour grade high strength, quenched and tempered steel weldments. *Inter J Hydrog Energy* 33(7):1897–1908
28. Yue X, Lippold JC, Alexandrov BT, Babu SS (2012) Continuous cooling transformation behavior in the CGHAZ of naval steels. *Weld J* 91(3):67s–75s
29. Yue X, Feng XL, Lippold JC (2013) Quantifying heat-affected zone hydrogen-induced cracking in high-strength naval steels. *Weld J* 92(9):265s–273s
30. Yue X, Feng XL, Lippold JC (2014) Effect of diffusible hydrogen level on heat-affected zone hydrogen-induced cracking of high-strength steels. *Weld World* 58(1):101–109
31. Yue X, Feng XL, Lippold JC (2014) Effect of welding parameters on the heat-affected zone hydrogen-induced cracking tendency of a blast-resistant steel. *Weld J* 93(3):98s–105s
32. Easterling K (1992) *Introduction to the physical metallurgy of welding*. Butterworth-Heinemann, Oxford, pp 12–15
33. Nawrocki JG, DuPont JN, Robino CV, Marder AR (2001) The postweld heat treatment response of simulated coarse-grained heat-affected zones in a new ferritic steel. *Metall Mater Trans A* 32:2585–2594
34. Spanos G, Fonda RW, Vandermeer RA, Matuszeski A (1995) Microstructural changes in HSLA-100 steel thermally cycled to simulate the heat-affected zone during welding. *Metall Mater Trans A* 26:3277–3293
35. Yue X, Lippold JC (2013) Evaluation of heat-affected zone hydrogen induced cracking in Navy steels. *Weld J* 92(1):20s–28s
36. Yue X, Feng XL, Lippold JC (2013) Strength increase in the coarse-grained heat-affected zone of a high-strength, blast-resistant steel after post-weld heat treatment. *Mater Sci Eng A* 585:149–154
37. Bhadeshia HKDH (2001) *Bainite in steels: transformations, microstructure and properties*. IOM, London, pp 63–75
38. Dickinson DW, Ries GD (1979) Implant testing of medium to high strength steel—a model for predicting delayed cracking susceptibility. *Weld J* 59(7):205s–211s